An Identification of the Mechanisms that Lead to Arctic Warming During Planetary-Scale and Synoptic-Scale Wave Life Cycles

CORY BAGGETT AND SUKYOUNG LEE

Department of Meteorology, The Pennsylvania State University, University Park, Pennsylvania

(Manuscript received 25 May 2016, in final form 9 March 2017)

ABSTRACT

The dynamical mechanisms that lead to wintertime Arctic warming during the planetary-scale wave (PSW) and synoptic-scale wave (SSW) life cycles are identified by performing a composite analysis of ERA-Interim data. The PSW life cycle is preceded by localized tropical convection over the western Pacific. Upon reaching the midlatitudes, the PSWs amplify as they undergo baroclinic conversion and constructively interfere with the climatological stationary waves. The PSWs flux large quantities of sensible and latent heat into the Arctic, which produces a regionally enhanced greenhouse effect that increases downward IR and warms the Arctic 2-m temperature. The SSW life cycle is also capable of increasing downward IR and warming the Arctic 2-m temperature, but the greatest warming is accomplished in the subset of SSW events with the most amplified PSWs. Consequently, during both the PSW and SSW life cycles, wintertime Arctic warming arises from the amplification of the PSWs.

1. Introduction

Baroclinic eddies have long been recognized as being important agents of atmospheric poleward heat transport, as they participate in the redistribution of excess solar energy that Earth gains at low latitudes to higher latitudes (Charney 1947; Eady 1949; Lorenz 1955; Peixoto and Oort 1992). A decomposition of the eddies in space and time reveals the importance of both the transient and stationary eddies in this poleward transport of sensible and latent heat [Figs. 13.6 and 12.12 of Peixoto and Oort (1992), respectively]. Interestingly, over the Northern Hemisphere during its winter, the maximum transport of sensible heat by the stationary eddies resides at ~55°N, farther north than the maximum transport by the transient eddies at ~40°N. A similar latitudinal displacement is seen for latent heat transport. Newman et al. (2012) decomposed moisture transport into synoptic- and low-frequency variability and similarly found that low-frequency variability has a leading influence over the Arctic.

To support these findings, we present Fig. 1 which displays the December–March (DJFM) climatological stationary waves of streamfunction and temperature as functions of longitude and pressure level along 65°N, near the southern periphery of the Arctic. (The data used to produce Fig. 1 is described in section 2.) The figure reveals a gentle westward tilt with height in the streamfunction field, indicative of the baroclinic nature of these stationary waves and their ability to transport heat poleward. We find that the poleward sensible heat transport is 1.17 PW throughout the entire column—a value in good agreement with previous studies (Peixoto and Oort 1992; Trenberth and Stepaniak 2003). Partitioning the transport between tropospheric (below 300 hPa) and stratospheric contributions, we find transports of 0.46 and 0.71 PW, respectively. Insomuch as there are mechanisms that excite transient planetary-scale waves that act to amplify through constructive interference these stationary planetary-scale waves (Garfinkel et al. 2010; Fletcher and Kushner 2011; Smith et al. 2010; Goss et al. 2016), it is reasonable to expect that these mechanisms would produce enhanced values of poleward heat transport (Lee 2014). In fact, by partitioning atmospheric waves by horizontal scale into planetary- and synoptic-scale components (k = 1–3 and $k \geq 4$, respectively), Baggett and Lee (2015, hereafter BL15) showed that the contribution of the planetary-scale waves (PSW) to latent and sensible heat flux convergence (HFC) over the Arctic dominates over the contribution by the synoptic-scale waves (SSW) during DJFM.

Corresponding author: Cory Baggett, cbaggett@rams.colostate.edu

DOI: 10.1175/JAS-D-16-0156.1

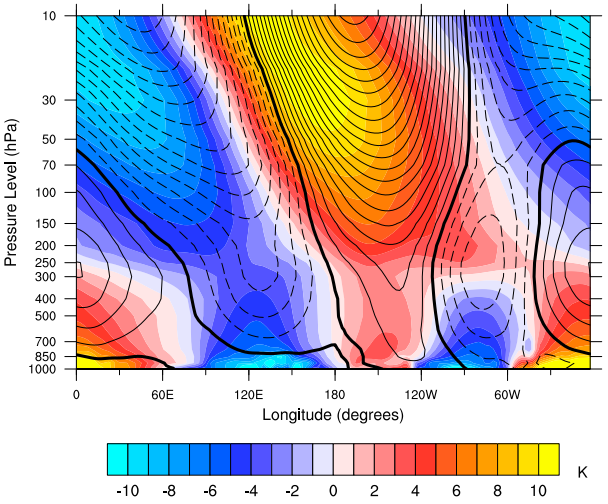

FIG. 1. DJFM climatological stationary waves of temperature (shading) and streamfunction (contours) as a function of longitude and pressure level along 65°N. Solid (dashed) contours indicate positive (negative) values, the zero contour is in bold, and the contour interval is $3 \times 10^6\,\mathrm{m^2\,s^{-1}}$. Evaluated from ERA-Interim (1979–2014) data.

Together with BL15, Baggett et al. (2016, hereafter B16) found that the PSW life cycle grows and decays following localized tropical convection over the Maritime Continent, constructively interferes with the climatological stationary waves, and results in Arctic warming greater than that seen during a separately identified SSW life cycle. Despite this broad dynamical depiction, these studies left some key dynamical processes unexplored that we plan to investigate in this study. These processes include 1) the possibility of a tropical influence on the SSW life cycle and how it compares to the previously explored tropical influence on the PSW life cycle, 2) an investigation of stratosphere–troposphere interactions which are known to be more likely when the PSWs are amplified (Garfinkel et al. 2010; Fletcher and Kushner 2011; Smith et al. 2010), 3) the contrasting roles of planetary- and synoptic-scale heat fluxes into the Arctic during each life cycle, and 4) the influence of these fluxes in developing a regionally enhanced greenhouse effect over the Arctic. Furthermore, although BL15 found that Arctic warming was greater during the PSW life cycle than the SSW life cycle, the potential influence of PSW activity during the SSW life cycle was not considered. Neglecting to sort the SSW events by PSW activity is perhaps nontrivial as the two spatial scales are known to coexist and interact (e.g., Benedict et al. 2004; Franzke et al. 2011). In fact, it is entirely plausible that there is a bin of SSW events with enhanced PSW activity that is largely responsible for the warming in the Arctic seen in the composite of all SSW events—the principal hypothesis we intend to address in this study.

An additional intriguing aspect of the PSW life cycle found by BL15 is that the PSWs grow in the presence of a nonenhanced equator-to-pole 2-m temperature gradient and anomalously low values of hemispheric zonal available potential energy (ZAPE; Lorenz 1955). This contrasts with the SSW life cycle whose peak amplitude is preceded by both a significantly enhanced equator-to-pole 2-m temperature gradient and ZAPE. Rather than conforming to the usual flux–gradient relationship, the PSWs are forced by localized tropical convection and grow further as they tap ZAPE in the midlatitudes. This property of the PSW life cycle differs from the "dynamical amplifier theory" by Cai (2005) and its extension (Cai 2006; Cai and Lu 2007; Lu and Cai 2010; Wu et al. 2011; Cai and Tung 2012; Zelinka and Hartmann 2012), which was proposed to explain Arctic amplification of the surface temperature. It states that in a warmer climate, the equator-to-pole upper-tropospheric temperature gradient increases. In response, poleward heat transport by baroclinic eddies is enhanced, and the resulting warming of the Arctic air in turn warms the surface through radiation. Although the theory was proposed to explain long-term climate changes, baroclinic eddy fluxes typically occur at intraseasonal time scales of ~1–2 weeks. Therefore, we ask the following question: Are the PSW and SSW life cycles consistent with the dynamical amplifier theory?

We organize this paper as follows: section 2 describes the data and methods used to answer the aforementioned questions, section 3 provides our results, and section 4 concludes the study and provides a summary table listing the notable characteristics of the PSW and SSW life cycles.

2. Data and methods

This study is an extension of BL15 and B16, which left unexplored some of the key dynamical mechanisms that lead to Arctic warming during both the PSW and SSW life cycles. Therefore, for consistency, we use the same data source and similar analysis techniques as BL15, which we briefly reiterate below. Furthermore, we adopt the nomenclature and initialisms that were established in B16.

From the European Centre for Medium-Range Weather Forecasts (ECMWF) interim reanalysis (ERA-Interim) project (Dee et al. 2011; ECMWF 2009), we obtain daily 0000 UTC data (1979–2014) of zonal wind u, meridional wind v, vertical velocity ω ($\mathrm{Pa\,s^{-1}}$),

specific humidity q, temperature T, 2-m temperature (2MT), outgoing longwave radiation (OLR), total column water (TCW), downward infrared radiation (IR), and potential temperature θ on the 2 potential vorticity unit (PVU; $1\,\text{PVU} = 10^{-6}\,\text{m}^2\,\text{s}^{-1}\,\text{K}\,\text{kg}^{-1}$) surface $\theta_{2\text{PVU}}$. All of the data have a horizontal resolution of 2.5° × 2.5°, while u, v, ω, q, and T have a fourth dimension in the vertical comprising 23 pressure levels between 1000 and 1 hPa.

To identify PSW and SSW life cycle events, we use daily values of eddy kinetic energy (EKE) integrated over the Northern Hemisphere. We calculate EKE for PSWs (SSWs) by performing a Fourier analysis in the longitudinal direction on u and v and calculating the contributions by zonal wavenumbers k = 1–3 ($k \geq 4$). The growth and decay of EKE within their respective time series is used to infer PSW and SSW life cycle events (BL15). To isolate events within the two time series, we calculate anomalous values of EKE by subtracting the calendar-day mean, of which we retain only the first two harmonics of its raw annual cycle. Events are isolated by first identifying days when EKE exceeds a threshold of one standard deviation, calculated during DJFM only. Then from these days, we pick the day that has the highest value of EKE within a 14-day time period. This procedure yields 102 PSW events and 133 SSW events.

Next, we create three bins of SSW events by ranking them according to the magnitude of the PSW EKE averaged over lag days −3 to +3 during each event. To test the sensitivity of our results to the lag days we average, we bin the events based on lag day 0 only and based on the averages during lag days −6 to 0 and 0 to +6 and find that our results remain qualitatively unchanged. Our analysis focuses on the top and bottom third of events which we denote as P+|S for SSW events with high PSW activity and P−|S for SSW events with low PSW activity. These bins contain 44 events each. By construction, there is no guarantee that either bin has greater SSW activity than the other. In addition, we analyze the top of three bins of PSW events ranked by the magnitude of PSW EKE averaged over lag days −3 to +3 during each event. We denote this bin P+|P, and it contains 34 events.

Having separated the PSW and SSW life cycle events into bins, we analyze them by performing a composite analysis of the anomalous values of various atmospheric variables including the following: planetary-scale and synoptic-scale EKE, baroclinic conversion (BC), sensible HFC, and latent HFC. We also composite ZAPE, 2MT, OLR, streamfunction, TCW, and downward IR. The energetic terms (EKE, BC, and ZAPE) are derived from the equations in Peixoto and Oort (1974). In addition, we calculate anomalous wave activity flux and its divergence through Eliassen–Palm (E-P) flux diagnostics (Edmon et al. 1980) to diagnose the source and sinks of wave activity and its influence on the mean flow. In the region where E-P flux diverges (converges), the eddies accelerate (decelerate) the zonal-mean zonal wind $\overline{u}$. Again, the E-P flux and its divergence are separated into planetary- and synoptic-scale components.

Finally, we consider the possibility that the PSWs we identify during these life cycles could in fact be SSWs in the midlatitudes that propagate northward, conserve their wavelength, and mathematically transform into PSWs. We refer the reader to B16, where we argue against this. We repeat some of those arguments here. Although our analysis cannot completely rule out a latitudinal transformation in wavenumber, it is wavenumber (not wavelength) that is generally conserved as waves propagate northward. Moreover, SSWs reach their turning latitude and return equatorward before reaching the Arctic (Hoskins and Karoly 1981). Rather than a latitudinal transformation in wavenumber, B16 showed that the SSWs present in the North Pacific during the PSW life cycle undergo Rossby wave breaking near 60°N (Fig. 7a of B16). Essentially, the PSW life cycle meridionally amplifies the planetary-scale steering flow. As a result of this meridional amplification, the SSWs are steered much farther north, where they undergo Rossby wave breaking, further amplifying the PSWs. Through this process, not only can the PSWs contribute to heat transport into the Arctic, their meridional amplification steers the SSWs and their attendant atmospheric rivers northward where they can also contribute to Arctic warming by further amplifying the PSWs and providing abundant moisture to the region.

Moreover, we calculate (not shown here) anomalous EKE as a function of lag day, latitude, and all wavenumbers. If SSWs are in fact mathematically transforming into PSWs, then one would expect to see enhanced SSW EKE that propagates northward in time, acquiring planetary-scale wavenumbers. Instead, we find that PSW EKE exists well in advance of any enhanced SSW EKE in the midlatitudes and spatially subsumes the entire extratropics during both the P+|P and P+|S life cycles. With respect to P+|S life cycle, we observe a northward propagation of SSW EKE to ~60°N where it merges with the preexisting PSW EKE signal. This merging poses some ambiguity as to whether or not the SSWs are experiencing a latitudinal transformation in wavenumber. However, we contend this transformation is less likely than the SSWs either reaching their turning latitude or undergoing wave breaking as they propagate northward (Hoskins and Karoly 1981; B16).

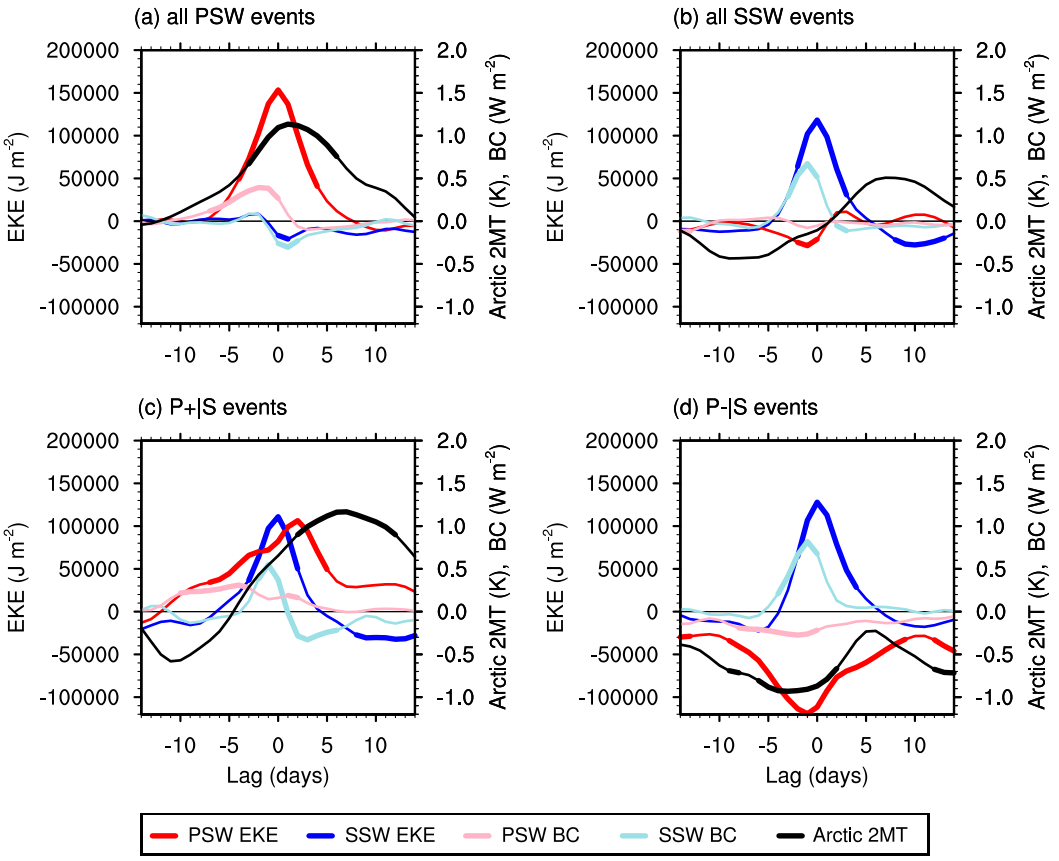

FIG. 2. Composites of anomalous values of PSW EKE (red), SSW EKE (blue), PSW BC (light red), SSW BC (light blue), and Arctic 2MT (black) during (a) all PSW, (b) all SSW, (c) P+|S, and (d) P−|S events (n = 102, 133, 44, and 44, respectively). EKE and BC are vertically integrated over all pressure levels and area averaged over the Northern Hemisphere. Arctic 2MT is area averaged north of 65°N. A two-sided Student's t test is used to determine statistical significance at the 5% level, as indicated by thick line segments. Two iterations of a 1–2–1 smoothing scheme are applied before plotting. Evaluated from ERA-Interim (1979–2014) data.

3. Results

a. Energetics

Our analysis begins by comparing and contrasting values of EKE, BC, and Arctic 2MT observed during the PSW and SSW life cycles during DJFM. To calculate the Arctic 2MT, we area average the 2MT north of 65°N, whereas both EKE and BC are vertically integrated over all pressure levels and area averaged over the entire Northern Hemisphere. In addition, we decompose EKE and BC into their PSW and SSW components.

Figure 2a depicts the composite of all PSW events. It reveals that the peak in PSW EKE is preceded by an Arctic that is anomalously warm. At short negative lags, PSW BC grows, converting ZAPE into eddy available potential energy (Lorenz 1955; BL15). Presumably, as a result of the poleward heat fluxes that occur during PSW BC, the Arctic warms to ~1.2°C above normal at lag day +1 and remains anomalously warm. We also notice that SSW BC and EKE are small, which suggests that the SSWs play less of a role in poleward heat flux into the Arctic during this life cycle. An investigation of these heat fluxes will be provided in section 3c (Fig. 10). Also, in section 3c, we will examine the zonal-mean anomalies of the quantities depicted in Fig. 2 through latitude–lag day plots (Fig. 6).

Now, we turn our attention to the composite of all SSW events (Fig. 2b). We see a more traditional eddy life cycle that commences with an anomalously cold Arctic 2MT that is followed by maxima in SSW BC at lag day −1 and SSW EKE at lag day 0. During the life cycle both PSW BC and EKE are near normal values. During this life cycle, the Arctic 2MT warms by ~1.0°C, reaching values ~0.5°C above normal. One would presume that the SSW activity and its associated heat fluxes are responsible for warming the Arctic. However, we will present evidence shortly that this may not be the case. Regardless, Figs. 2a and 2b corroborate the results

of BL15, where it was shown that the PSW life cycle leads to a warmer Arctic than the SSW life cycle despite the PSW life cycle having lower values of ZAPE and a weaker equator-to-pole 2MT gradient.

Figures 2c and 2d depict two bins of SSW events based on PSW EKE. The P+|S life cycle depicts a maximum in PSW EKE that follows a maximum in SSW EKE (Fig. 2c). Each maximum in EKE is preceded by their respective peaks in BC. Throughout the life cycle, the Arctic 2MT begins below normal, warms by ~1.8°C, and reaches a maximum value of ~1.2°C by lag day +7. Turning our attention to the P−|S life cycle (Fig. 2d), we again see that the maximum in SSW EKE is preceded by a maximum in SSW BC. However, as expected by the nature of the composite, PSW EKE and BC are anomalously negative throughout the life cycle. Although the Arctic 2MT warms by ~0.8°C near the peak of the life cycle, it never exceeds normal at any lag day.

We conclude our discussion of Fig. 2 by noting that the warming the Arctic experiences during the P−|S life cycle (~0.8°C) is much less than the warming that takes place during the P+|S life cycle (~1.8°C). The conclusion we draw from this result is that the PSWs are paramount for warming the Arctic during both the PSW and SSW life cycles. Although every life cycle warms the Arctic, the least warming occurs during the P−|S life cycle, when the PSWs are not amplified. In the following sections, we will attempt to provide further evidence to buttress this conclusion by focusing on three particular life cycles: P+|P, P+|S, and P−|S. We chose to examine the P+|P life cycle rather than the PSW life cycle comprising all events because the smaller composite of 34 events yields clearer results with larger magnitudes, while remaining statistically significant and qualitatively similar to the larger sample. We begin our analysis of these three life cycles by first examining tropical convection and its role in exciting the PSW life cycle.

b. *Tropical convection and Rossby wave response*

To examine tropical convection, we employ Hovmöller diagrams of OLR that is averaged between 15°S and 15°N (Hovmöller 1949). Negative (positive) OLR anomalies correspond to enhanced (suppressed) tropical convection. Figure 3a reveals that throughout the P+|P life cycle, convection is suppressed near 180° over the central Pacific and enhanced to the west over the western Pacific and Maritime Continent. This pattern suggests that the P+|P life cycle occurs more frequently during seasons with a vigorous Walker Circulation and an active La Niña. To confirm this finding, we count the number of P+|P events that occur during either El Niño, La Niña, or neutral conditions [the caption to Table 1 provides El Niño–Southern Oscillation (ENSO) classification criteria]. Indeed, Table 1 reveals that P+|P events occur 15 times each during La Niña and neutral conditions while only occurring four times during El Niño. Embedded in this La Niña signal, convection over the Maritime Continent translates eastward over the western Pacific during negative lags, reminiscent of a propagating Madden–Julian oscillation (MJO; Madden and Julian 1971, 1972). To verify this propagation, we composite in Fig. 4 the real-time multivariate MJO

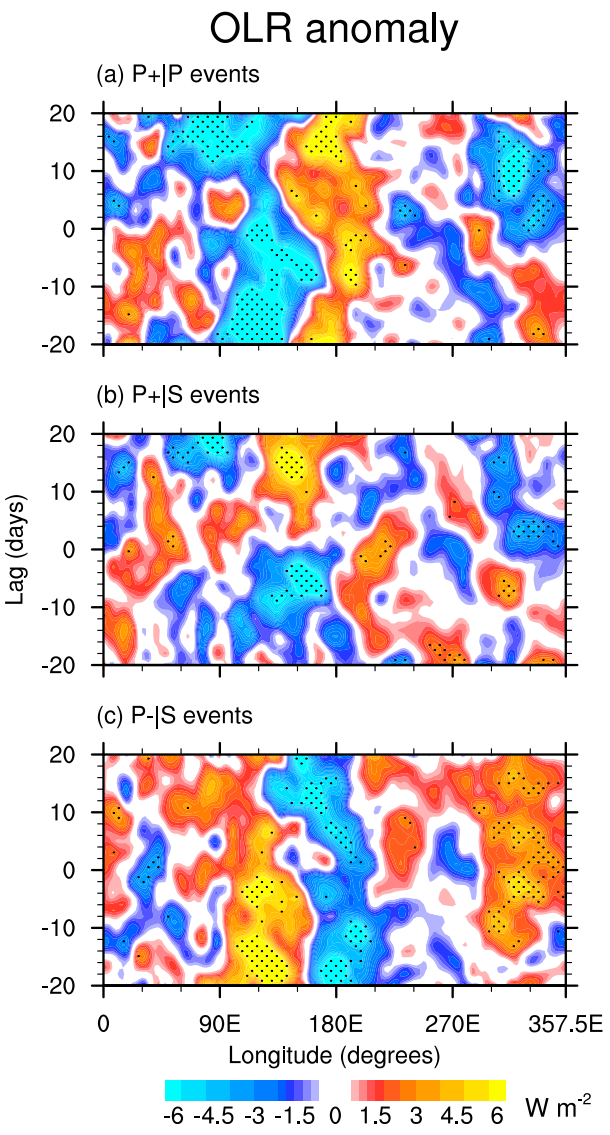

FIG. 3. Hovmöller diagrams of anomalous OLR composited during (a) P+|P, (b) P+|S, and (c) P−|S events (n = 34, 44, and 44, respectively). OLR is averaged, weighted by cosφ, between 15°S and 15°N. A Monte Carlo simulation with 1000 random samples is used to determine statistical significance at the 5% level, as indicated by stippled areas. Two iterations of a nine-point local smoothing scheme are applied before plotting. Evaluated from ERA-Interim (1979–2014) data.

TABLE 1. Counts of P+|P, P+|S, and P−|S events according to their ENSO classification. In this study, ENSO is classified as El Niño (La Niña) when the 3-month running mean of sea surface temperature anomalies in the Niño-3.4 region are greater than 0.5°C (less than −0.5°C) for five sequential and overlapping 3-month periods (NOAA/NCEP/CPC 2016). Periods with neither an active El Niño nor La Niña are classified as neutral.

	Life cycle		
ENSO phase	P+|P	P+|S	P−|S
El Niño	4	11	17
La Niña	15	12	6
Neutral	15	21	21

indices, RMM1 and RMM2, on a phase space diagram (Wheeler and Hendon 2004; BOM 2016). From Fig. 4, it is evident that the P+|P life cycle is associated with an MJO that transitions through phases 4, 5, and 6 during negative lags.

This result supports the findings of both Lee (2012) and Yoo et al. (2012a,b), where it was shown that La Niña and phase 5 of the MJO, respectively, favor Arctic warming. In fact, idealized modeling studies have confirmed that a heating anomaly over the Maritime Continent leads to the amplification of PSWs and Arctic warming (Yoo et al. 2012a; B16). More specifically, B16 perturbed the DJFM climatological background flow with heating that corresponds to the latent heat release produced by tropical convective precipitation at negative lags during the P+|P life cycle. In response to this heating, the pattern correlation between the anomalous 300-hPa streamfunction in the model and that observed at the peak of the P+|P life cycle reached 0.69 over the North Pacific by model day 14 (Fig. 9 of B16). While these model results are highly suggestive that anomalous tropical convection leads to an amplification of extratropical PSWs, we cannot dismiss the possibility that extratropical forcings may also cause their amplification and simultaneously produce anomalous tropical convection.

Figures 3b and 4 reveal that enhanced tropical convection exists at negative lags over the western Pacific during the P+|S life cycle, similar to the P+|P life cycle. However, unlike the P+|P life cycle, the P+|S life cycle does not have a preference for either La Niña or El Niño (12 and 11 events, respectively; Table 1). This highlights the importance of localized tropical convection over the Maritime Continent and western Pacific, a region ideally suited to create a Rossby wave source capable of producing a Rossby wave train over the North Pacific (Sardeshmukh and Hoskins 1988). This Rossby wave train arches through the North Pacific and North America, producing a ridge near Alaska and a trough in northeastern North America during both the P+|P and

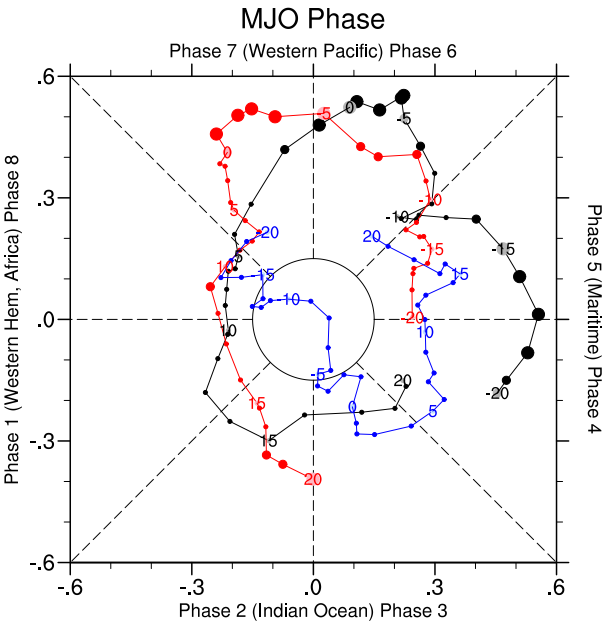

FIG. 4. Composites of RMM1 and RMM2 on a Wheeler and Hendon phase-space diagram during (a) P+|P (black), (b) P+|S (red), and (c) P−|S (blue) events (n = 34, 44, and 44, respectively). Individual lag days are indicated by circles and labeled every 5 days. A two-sided Student's t test is used to determine statistical significance. Large (medium) circles indicate that either RMM1 or RMM2 at a particular lag day is significant at the 5% (10%) level.

P+|S life cycles (Figs. 5a,c). The anomalous streamfunction associated with this ridge–trough dipole constructively interferes with the climatological DJFM stationary waves (Figs. 5a,b,c,d). To quantify the degree of constructive interference that occurs, we calculate the projection over the Northern Hemisphere of the anomalous waves onto the stationary waves using Eq. (1) of Goss et al. (2016). The projection values are positive and statistically significant at the 5% level at the peak of each life cycle (not shown here). The timing of the maximum response in the streamfunction is consistent with the ~10 days that Rossby waves need to propagate from the tropics to the high latitudes (Hoskins and Karoly 1981). Moreover, while the PSWs initially amplify through forcing by tropical convection, they subsequently are further amplified through PSW BC in the midlatitudes (Figs. 6c,h). We wish to emphasize here that these PSWs are not the product of baroclinic instability (BL15; Lee 2014). Rather, these PSWs are vertically propagating Rossby waves that tilt upward and poleward with height and are capable of transporting heat poleward (Charney and Drazin 1961) through baroclinic conversion, thereby consuming ZAPE that is left untapped by unstable baroclinic waves.

Tropical convection during the P−|S life cycle (Fig. 3c) contrasts sharply with the P+|P life cycle. The

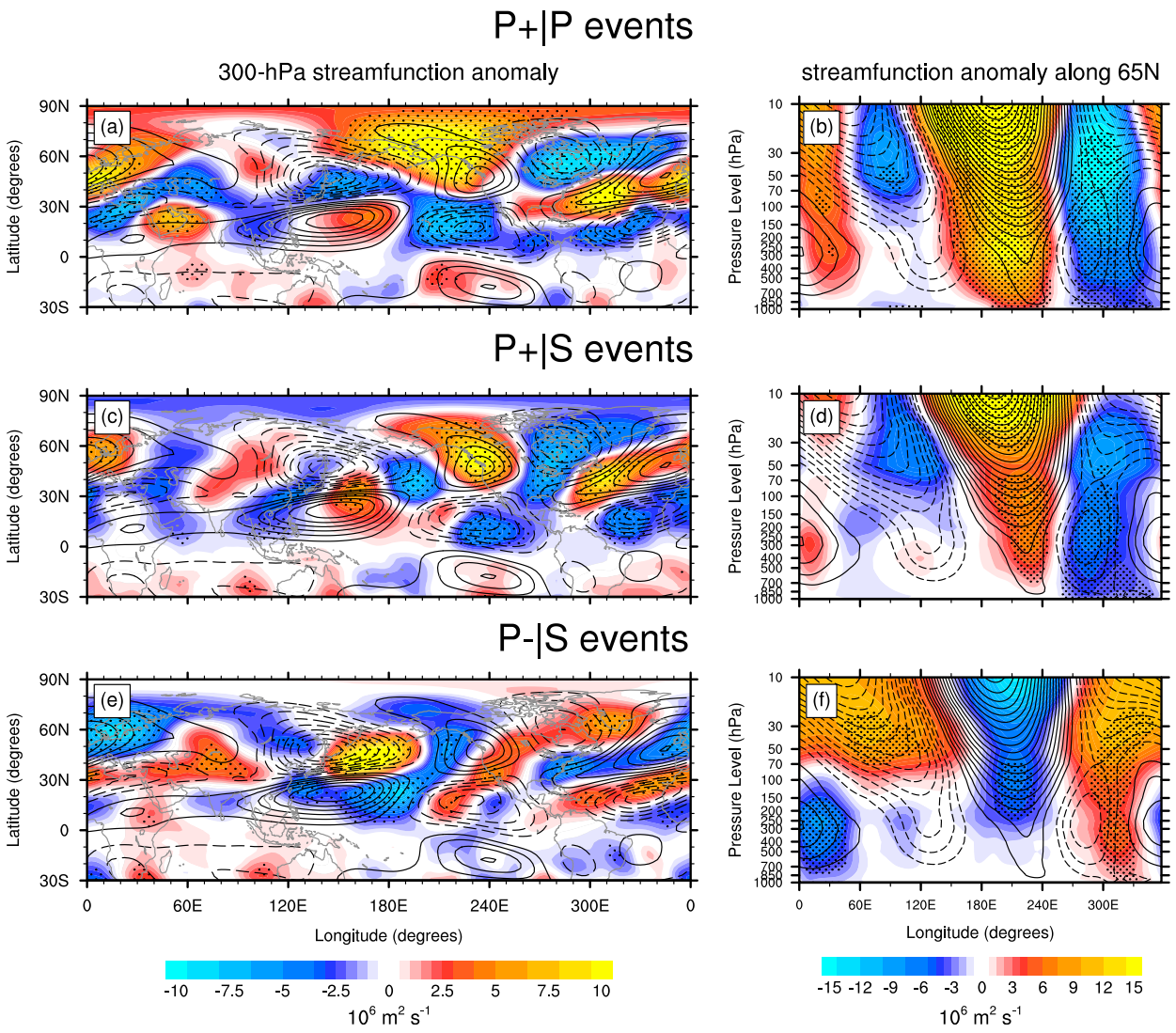

FIG. 5. Composites of anomalous streamfunction during (a),(b) P+|P, (c),(d) P+|S, and (e),(f) P−|S events (n = 34, 44, and 44, respectively), averaged over lag days −1 to +1 of each life cycle. Here, (a),(c), and (e) depict the streamfunction at 300 hPa while (b),(d), and (f) depict the streamfunction along 65°N. Solid (dashed) black contours indicate positive (negative) values of the DJFM climatological stationary wave of streamfunction. The contour interval is 3×10^6 m^2 s^{-1}, and the zero contour is omitted. A Monte Carlo simulation with 1000 random samples is used to determine statistical significance at the 5% level, as indicated by stippled areas. Evaluated from ERA-Interim (1979–2014) data.

OLR pattern reveals enhanced (suppressed) tropical convection over the central (western) equatorial Pacific, indicating P−|S events tend to occur during El Niño (17 events) rather than La Niña (six events; Table 1). Moreover, Fig. 4 reveals that the MJO is suppressed at negative lags and statistically insignificant throughout the entire P−|S life cycle. Therefore, we conclude that P−|S events preferentially occur during El Niño during inactive periods of the MJO. The suppressed convection over the western Pacific and Maritime Continent likely serves as an anomalously positive Rossby wave source that excites a Rossby wave train that destructively interferes with the DJFM climatological stationary waves over the North Pacific, as evidenced by streamfunction fields at the peak of the life cycle (Figs. 5e,f). When we calculate the projection of the anomalous waves onto the stationary waves at the peak of the P−|S life cycle, we find it is negative and statistically significant at the 5% level.

c. *E-P flux diagnostics*

We now utilize E-P flux diagrams during each life cycle to examine the sources and sinks of both PSW and SSW activity and their influence on the mean flow

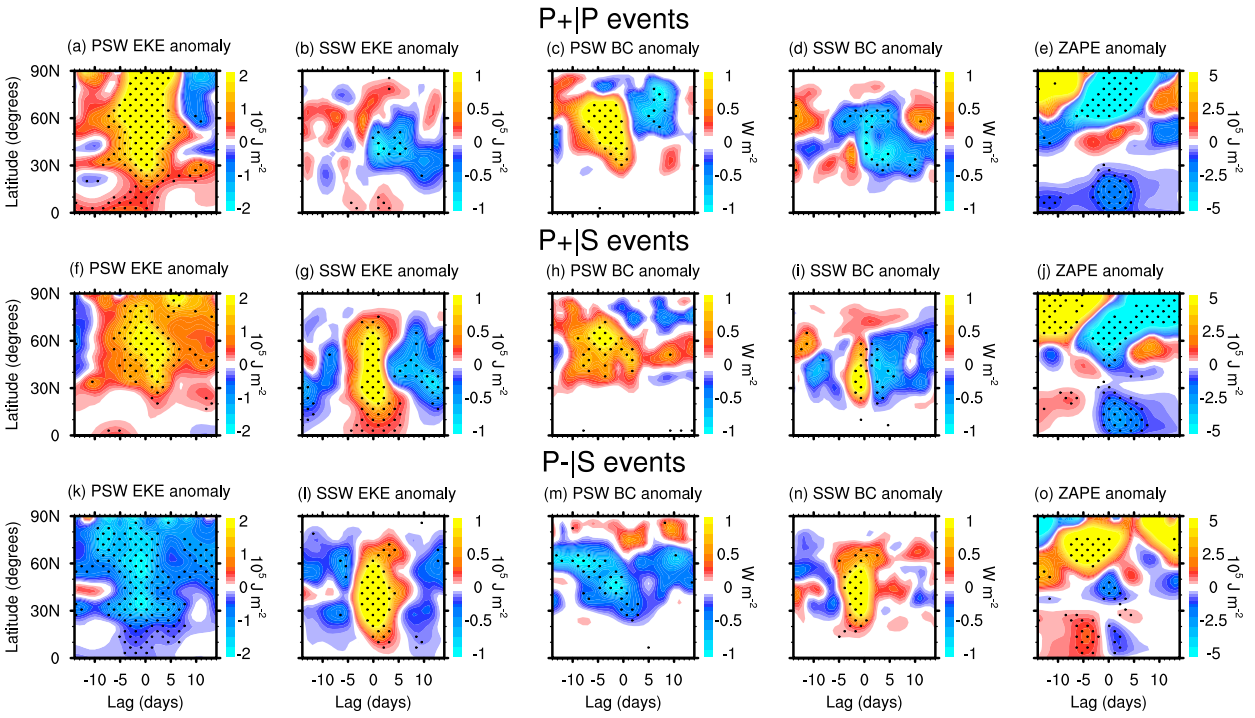

FIG. 6. Composites of the zonal means of anomalous (a),(f),(k) PSW EKE, (b),(g),(l) SSW EKE, (c),(h),(m) PSW BC, (d),(i),(n) SSW BC, and (e),(j),(o) ZAPE during (a)–(e) P+|P, (f)–(j) P+|S, and (k)–(o) P−|S events (n = 34, 44, and 44, respectively). A Monte Carlo simulation with 1000 random samples is used to determine statistical significance at the 5% level, as indicated by stippled areas. Two iterations of a nine-point local smoothing scheme are applied before plotting. Evaluated from ERA-Interim (1979–2014) data.

through their fluxes of momentum and sensible heat (Figs. 7–9). For each figure, we plot anomalous E-P flux divergence (shading) and anomalous $\overline{u}$ (contours). Also, we overlay anomalous E-P flux vectors that have at least one component statistically significant at the 5% level. We scale the vectors before plotting and provide details of this scaling in the caption of Fig. 7.

During negative lags of the P+|P life cycle (Figs. 7a–c), we see poleward-propagating PSW activity exiting the tropics near the tropopause between the equator and 20°N in response to the stirring produced by localized convection, consistent with prior studies (Yoo et al. 2012b; Feldstein and Lee 2014). Further evidence of tropical excitation may be seen in Fig. 6a, which shows anomalous PSW EKE over the deep tropics at negative lags that begins to propagate northward near lag day −10. Concurrently, we see over the Arctic that anomalous $\overline{u}$ is westerly, particularly aloft where an enhanced stratospheric polar vortex resides. We find that this enhanced stratospheric polar vortex results from anomalous PSW momentum flux convergence in the stratosphere prior to lag day −15 (not shown here). Between lag days −5 and +1 and centered at ~60°N, upward-propagating PSW activity dominates throughout the troposphere and stratosphere, indicative of poleward PSW sensible heat fluxes (Figs. 7b,c). This agrees with the theoretical study of the vertical propagation of PSWs made by Charney and Drazin (1961), where it was found that vertical wave propagation is favored for waves with large wavelengths in a westerly $\overline{u}$ environment. Figures 7b–d reveal that the poleward sensible heat fluxes produced by the vertically propagating PSW activity acts to decelerate the polar vortex, causing an anomalously easterly $\overline{u}$ in the upper troposphere. The deceleration of $\overline{u}$ in the polar region acts to conserve total atmospheric angular momentum by balancing the acceleration of $\overline{u}$ seen over the tropics (cf. Figs. 7a,b). Moreover, by thermal wind balance, one would expect an adjustment to the mean meridional circulation that would adiabatically warm the Arctic via anomalous sinking motions to the north of this deceleration (e.g., Lee 2012; Yoo et al. 2012b). By lag days +2 to +5, the presence of anomalous PSW momentum flux convergence would act to reaccelerate the stratospheric polar vortex (Fig. 7d).

The existence of vertically propagating PSW activity shows that PSW BC operates during the P+|P life cycle. However, the PSWs do not appear to be the result of baroclinic instability (BL15). Rather, zonally asymmetric heating over the tropics excites the PSWs, which

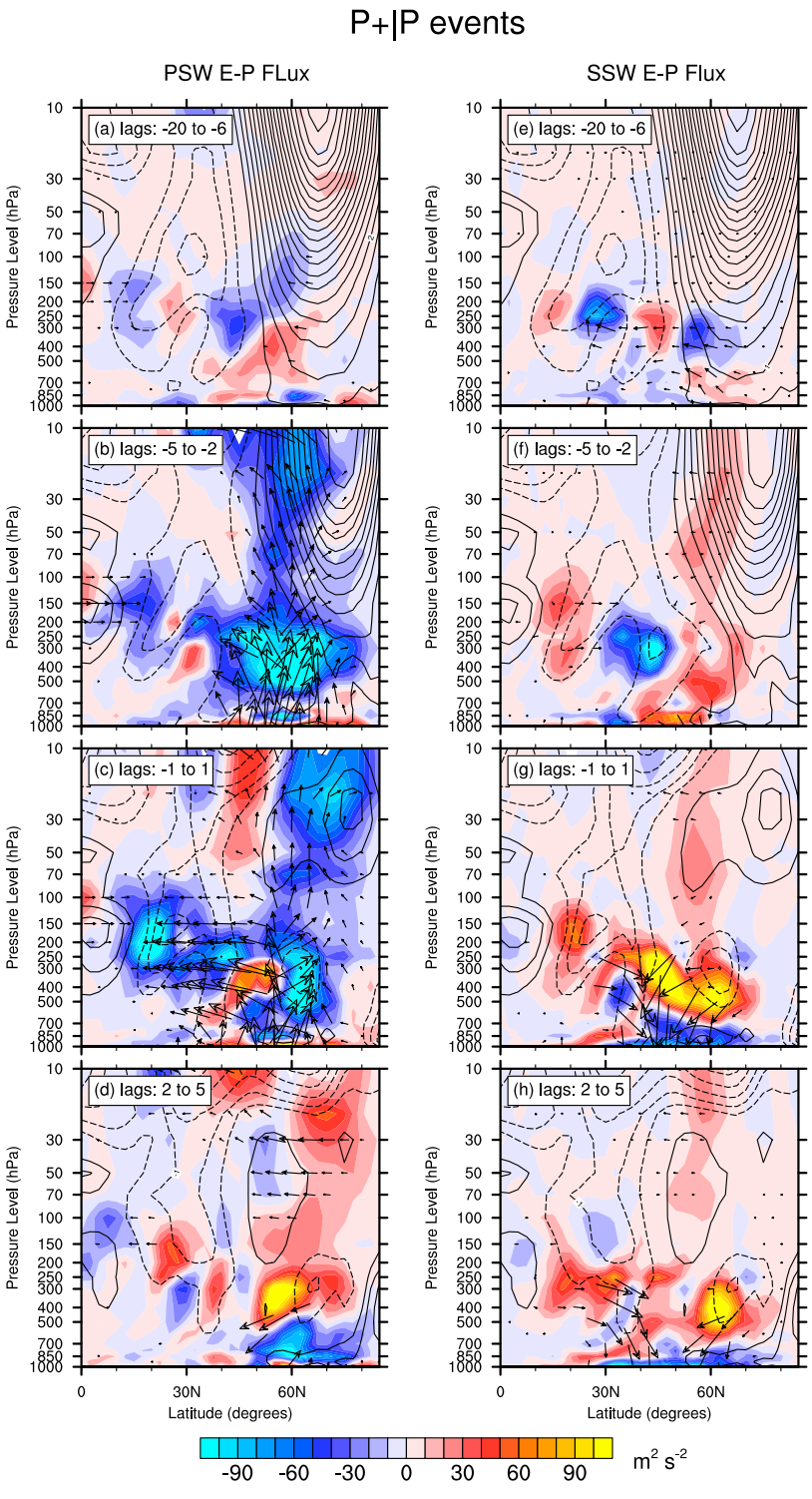

FIG. 7. Composites of anomalous (a)–(d) PSW and (e)–(h) SSW E-P flux vectors (F_φ, F_p) and their divergence (shading) during P+|P events ($n = 34$), averaged over selected lag days as indicated in each panel. The vectors are scaled before plotting by multiplying F_φ by $(a\pi)^{-1}$ and F_p by $10^{-5}\cos\varphi$. Furthermore, both F_φ and F_p are multiplied by $[\ln(100\,000p^{-1}) + 1]$ to allow visualization of the vectors in the stratosphere. Solid (dashed) black contours indicate positive (negative) anomalies of $\overline{u}$. The contour interval is 0.5 m s^{-1}, and the zero contour is omitted. E-P flux vectors are only plotted if either F_φ or F_p is statistically significant at the 5% level, as determined by a Monte Carlo simulation with 1000 random samples. Evaluated from ERA-Interim (1979–2014) data.

subsequently grow via PSW BC in the mid- and high latitudes by tapping ZAPE (Figs. 6a,c,e; Yoo et al. 2012a,b; BL15; B16). In contrast to the robust baroclinic life cycle exhibited by the PSWs, SSW activity is muted throughout the P+|P life cycle (Figs. 7e–h and 6b,d). Moreover, anomalous E-P flux vectors point downward, indicative of anomalously low SSW sensible HFC in the high latitudes (as confirmed in Fig. 10b; Fig. 10d displays a similar pattern in SSW latent HFC). In contrast to the SSWs, the vertically propagating PSW activity produces anomalously high PSW sensible and latent HFC over the Arctic (Figs. 10a,c). Interestingly, the vertically propagating PSW activity subsumes the SSW activity by simultaneously occurring over a broader range of latitudes (cf. Figs. 7c,g).

During the P+|S life cycle, the PSW activity shares many of the same features as during the P+|P life cycle (cf. Figs. 7a–d and 8a–d). We see PSW activity exiting the tropics near the tropopause between the equator and 20°N (Figs. 8a,b), which is consistent with the presence of localized tropical convection observed during negative lags (Fig. 3b), upward-propagating wave activity throughout the troposphere and stratosphere centered at ~60°N during lag days −5 to +1 (Figs. 8b,c), and a deceleration of the polar vortex due to poleward PSW sensible heat fluxes throughout the life cycle (Figs. 8a–d). In contrast to the muted SSW activity during the P+|P life cycle, the P+|S life cycle shows a more canonical baroclinic SSW life cycle with baroclinic conversion followed by barotropic decay (Figs. 8f,g). Figures 6g, 6i, and 6j show that this SSW activity is driven by SSW BC by tapping ZAPE in the low and midlatitudes, whereas the PSW activity grows through PSW BC in the mid- and high latitudes (Figs. 6f,h). The net result of the SSW activity is to decelerate $\overline{u}$ at ~25°N while accelerating $\overline{u}$ at ~50°N (cf. Figs. 8g,h). However, the PSW activity decelerates $\overline{u}$ near the tropopause at ~60°N (Figs. 8c,d), which could result in a meridional overturning circulation that contributes to warming the Arctic through adiabatic sinking motions. Regarding sensible and latent HFC, we find that both the PSWs and SSWs exhibit dipoles with anomalous divergence to the south and convergence to the north, straddling ~55° and ~30°N, respectively (Figs. 10e–h). We stress that although the SSW activity produces poleward transports of sensible and latent heat, the northward extent of these transports does not reach the Arctic, whereas the PSW fluxes do. Therefore, we conclude that the PSWs are more directly responsible for warming the Arctic during the P+|S life cycle.

With respect to the P−|S life cycle (Fig. 9), we observe that the PSW activity contrasts sharply with the P+|P and P+|S life cycles (cf. Figs. 7a–d, 8a–d, and 9a–d). Notably, we do not see any indication of wave activity leaving the tropics nor an acceleration of $\overline{u}$ in the upper troposphere over the equator (Figs. 9a,b). In the Arctic, we see an anomalously weak polar vortex in both the troposphere and the stratosphere. In the midlatitudes, the anomalous PSW activity is directed downward, centered at ~50°N, indicating muted PSW BC (Figs. 6k,m) and poleward sensible heat fluxes (Figs. 9b,c). In fact, the reduction in poleward sensible heat fluxes allows the Arctic to cool, which in turn accelerates the polar vortex during the life cycle (Figs. 9a–d). Similar to the P+|S life cycle, vigorous SSW activity exists during the P−|S life cycle (Figs. 9f,g) and grows in the midlatitudes through SSW BC as it taps ZAPE (Figs. 6l,n,o). We observe upward-propagating SSW activity centered at ~50°N, diverging from the surface and accelerating the near-surface westerlies. Simultaneously, this wave activity converges in the upper troposphere, which decelerates the upper-tropospheric eddy-driven jet at ~40°N (Fig. 9f). At the peak of the life cycle, the SSW activity turns equatorward (Fig. 9g). The associated eddy momentum fluxes reaccelerate and shift poleward the upper-tropospheric eddy-driven jet while decelerating the subtropical jet through barotropic processes (cf. Figs. 9e,g). Interestingly, because the vertically propagating PSW and SSW activity reside near the same latitude, are directed opposite of each other, and have nearly the same magnitude, they mostly cancel each other out, resulting in very little anomalous poleward sensible heat flux during the P−|S life cycle. Indeed, Figs. 10i and 10k reveal that anomalously low PSW sensible and latent HFC exist throughout the life cycle over the Arctic. However, a pulse of anomalously high SSW sensible and latent HFC impinge on the southern periphery of the Arctic near lag day 0 (Figs. 10j,l). Therefore, what Arctic warming occurs during the P−|S life cycle may be solely attributed to the SSW activity. Moreover, the lack of PSW activity dampens the Arctic warming by the SSWs to the extent that the Arctic 2MT remains below normal throughout the life cycle (Fig. 2d).

d. Localized greenhouse effect

Figures 10c and 10g shows that widespread latent HFC occurs over the Arctic during the P+|P and P+|S life cycles. As water vapor condenses over the cold Arctic, it releases latent energy that warms the surrounding environment. Moreover, this condensation leads to cloud formation, which, together with the remaining noncondensed water vapor, enhances the greenhouse effect over the Arctic by absorbing and remitting downward longwave radiation that would have otherwise escaped through the top of the atmosphere.

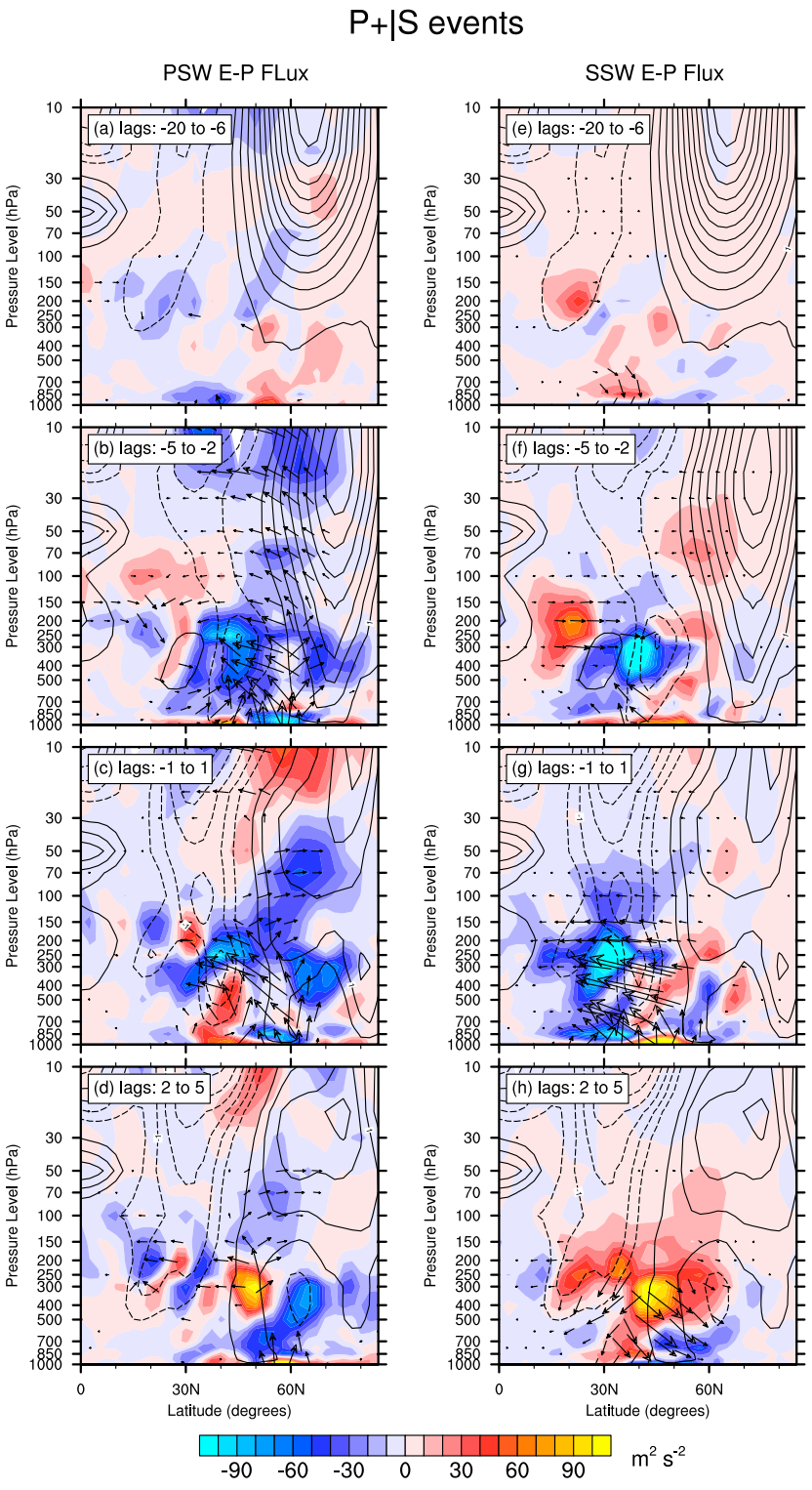

FIG. 8. As in Fig. 7, but for P+|S events (n = 44).

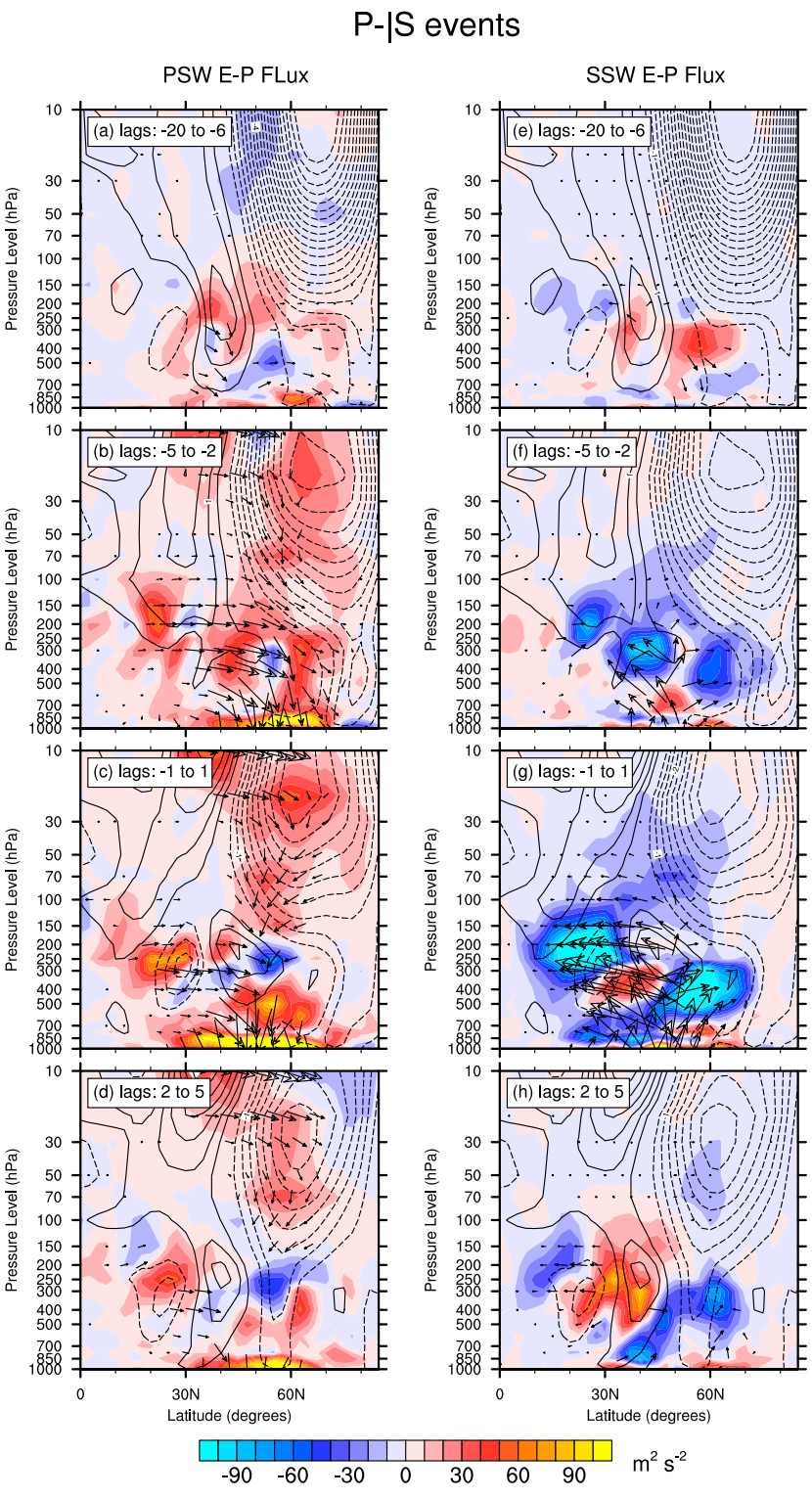

FIG. 9. As in Fig. 7, but for P−|S events (n = 44).

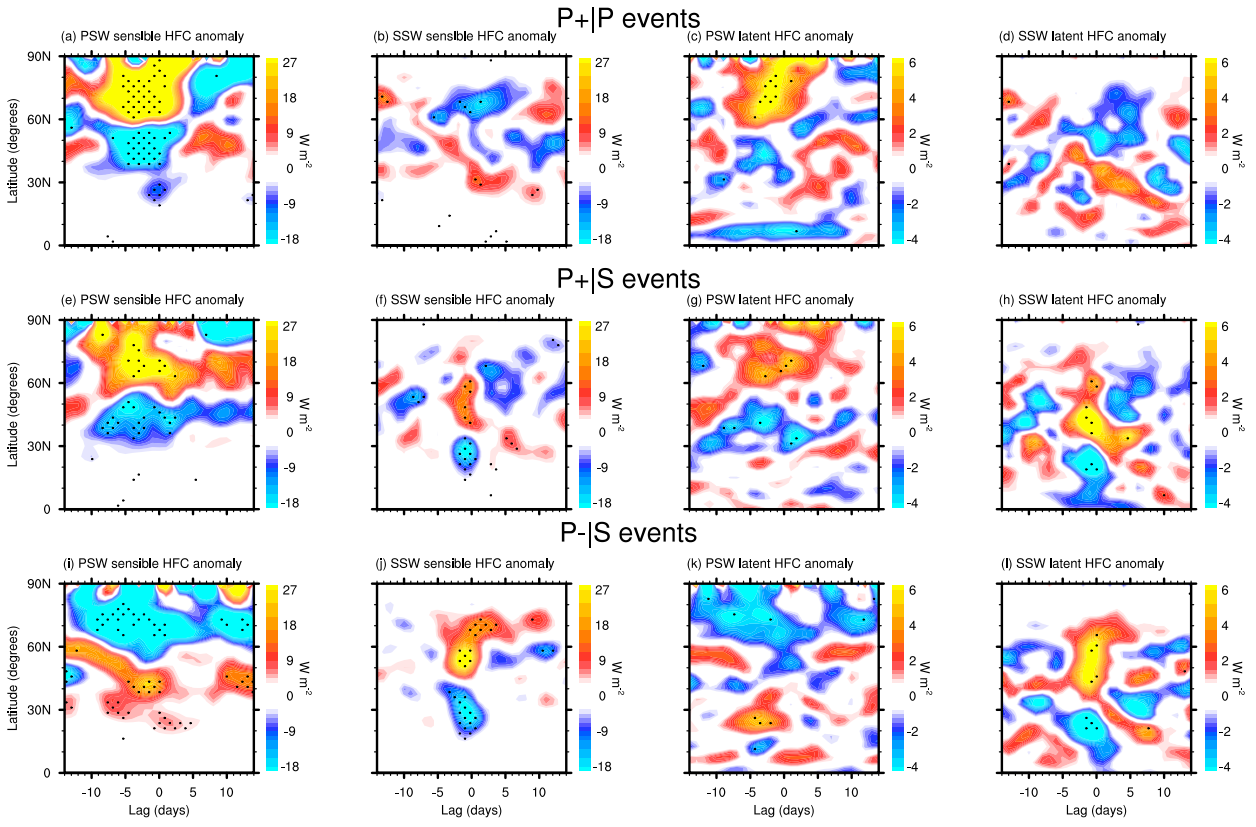

FIG. 10. Composites of the zonal means of anomalous (a),(e),(i) PSW sensible HFC, (b),(f),(j) SSW sensible HFC, (c),(g),(k) PSW latent HFC, and (d),(h),(l) SSW latent HFC during (a)–(d) P+|P, (e)–(h) P+|S, and (i)–(l) P−|S events ($n = 34$, 44, and 44, respectively). Sensible HFC is calculated according to $-\partial_y\left(c_p g^{-1}\int \overline{v_k T_k}\, dp\right)$, and latent HFC is calculated according to $-\partial_y\left(L_v g^{-1}\int \overline{v_k q_k}\, dp\right)$, where L_v is the latent heat of vaporization, c_p is the specific heat of air at constant pressure, g is the acceleration of gravity, and dp is the difference between reanalysis pressure levels. A Monte Carlo simulation with 1000 random samples is used to determine statistical significance at the 5% level, as indicated by stippled areas. Two iterations of a nine-point local smoothing scheme are applied before plotting. Evaluated from ERA-Interim (1979–2014) data.

Figures 11a–d display the zonal means of anomalous TCW, downward IR, OLR, and 2MT during the P+|P life cycle. It can be seen that anomalously high values of TCW develop over the southern Arctic near lag day −5 and progress northward through the peak of the life cycle. These high values of TCW may be attributed to anomalous PSW latent HFC (Fig. 10a). Interestingly, although SSW activity is not enhanced during the P+|P life cycle, B16 found that the most intense moisture transport from the subtropics to the Arctic is accomplished through the warm conveyor belts of synoptic-scale cyclones, which have been steered northward by the enhanced meridional component of the planetary-scale flow. This moisture transport, at lower latitudes than the Arctic, is often filamentary in structure, taking on the form of atmospheric rivers. As a result of enhanced poleward sensible and latent heat fluxes, the moist static energy of the Arctic atmosphere increases, which causes positive anomalies of both downward IR and OLR (Figs. 11b,c). The positive downward IR anomalies are highly correlated to the warm Arctic 2MT anomalies (Fig. 11d). Curiously, the positive OLR anomalies develop ~7 days after the development of the positive downward IR anomalies (cf. Figs. 11b,c). While beyond the scope of this study, this timing difference could be possibly attributed to anomalous cloud cover, their level, and their emission temperature.

Progressing to the second row of Fig. 11, the P+|S life cycle looks nearly identical to the P+|P life cycle, exhibiting similar values of anomalous TCW, downward IR, OLR, and 2MT (cf. Figs. 11a–h). One difference we note is that the greatest anomalies during the P+|S life cycle occur a few days after those during the P+|P life cycle, consistent with the maximum amplification of the PSWs occurring a few days after the SSWs during the P+|S life cycle (Fig. 2c). Finally, with respect to the P−|S life cycle, TCW, downward IR, and 2MT anomalies remain normal or below normal for all lags over the

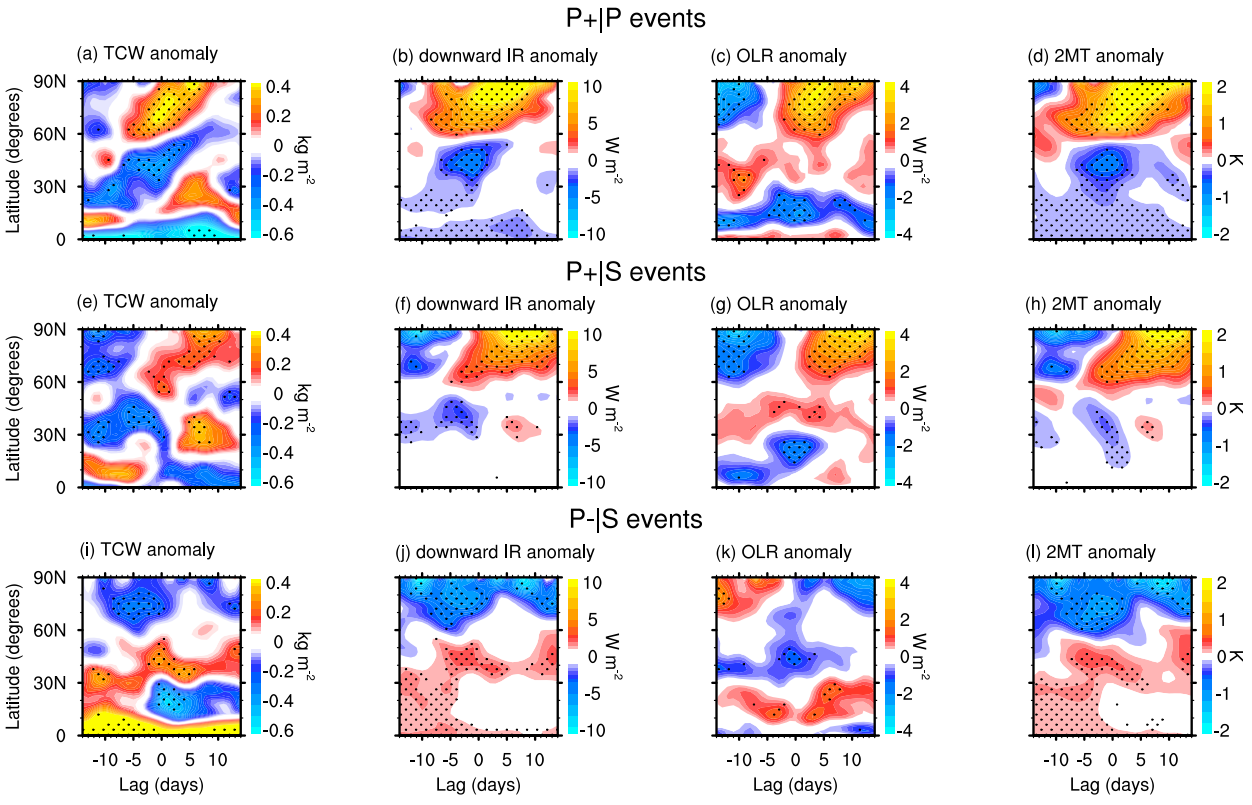

FIG. 11. Composites of the zonal means of anomalous (a),(e),(i) TCW, (b),(f),(j) downward IR, (c),(g),(k) OLR, and (d),(h),(l) 2MT during (a)–(d) P+|P, (e)–(h) P+|S, and (i)–(l) P−|S events (n = 34, 44, and 44, respectively). Positive (negative) anomalies of downward IR indicate enhanced downward (upward) radiation. Positive (negative) anomalies of OLR indicate enhanced upward (downward) radiation. A Monte Carlo simulation with 1000 random samples is used to determine statistical significance at the 5% level, as indicated by stippled areas. Two iterations of a nine-point local smoothing scheme are applied before plotting. Evaluated from ERA-Interim (1979–2014) data.

Arctic (Figs. 11i,j,l), while OLR anomalies are opposite of those seen during the P+|P and P+|S life cycles (cf. Figs. 11c,g,k). By comparing the P+|S to the P−|S life cycles, we conclude that the development of an enhanced localized greenhouse effect over the Arctic depends highly on the presence of amplified PSWs during the SSW life cycle.

e. *Dynamical amplifier theory*

Intriguingly, despite the reduced gradients in advance of the P+|P life cycle, it produces greater Arctic warming than the P−|S life cycle. We find this result compelling in the context of Arctic amplification. Namely, the PSWs deliver heat and moisture through baroclinic processes to very high latitudes without a reliance on the flux–gradient relationship. From the idea of turbulence closures, one would expect through a first-order closure of the flux–gradient relationship (Panofsky and Dutton 1984) a causality such that poleward heat fluxes would decrease in response to weakened gradients. An examination of Fig. 2 reveals that, relative to the SSW life cycle, the PSW life cycle is not reliant on this causality. From BL15 and the findings presented here, it is our contention that the PSWs are forced to tap ZAPE by localized tropical convection rather than being forced by baroclinic instability and an increased equator-to-pole 2MT gradient.

Using a simple four-box coupled atmosphere–surface radiative–transportive climate model, Cai (2005, 2006) also proposed that Arctic amplification can occur through enhanced poleward heat fluxes, a process coined by these studies as "the dynamical amplifier theory." Essentially, radiative forcing by enhanced greenhouse gases warms the troposphere over the tropics more than the high latitudes because of the warmer tropical surface. The extra warming over the tropics enhances the equator-to-pole upper-tropospheric temperature gradient, which in turn increases poleward heat transport through baroclinic eddies. Within the model, the baroclinic eddies are parameterized such that they respond linearly to the temperature difference between the two boxes in the upper layer [see Eq. (3) of Cai (2005)].

In effect, the model is constrained to obey the flux–gradient relationship. The poleward heat fluxes reduce the equator-to-pole upper-tropospheric temperature gradient, but not to the extent that it overwhelms the radiative forcing by the greenhouse gases. In the high latitudes, because of the coupling of the upper layer with the surface, radiative processes warm the surface layer more than in the tropics. This lessens the equator-to-pole 2MT as modeled by the temperature difference between the lower two boxes and results in Arctic amplification in the model. Cai (2005, 2006) found that reanalysis data and coupled global climate models showed that both the surplus of top of the atmosphere net radiation over the low latitudes and its deficit over the high latitudes increased. This was viewed as being consistent with an increase in the equator-to-pole upper-tropospheric temperature gradient.

The dynamical amplifier theory represents an equilibrium climatic state, and neither the PSW nor the SSW life cycles observed in this study are forced by greenhouse gases. However, as stated in the introduction, the baroclinic eddy fluxes that drive the dynamical poleward heat transport within the theory typically occur during eddy life cycles that operate at intraseasonal time scales of ~1–2 weeks. Therefore, we ask the following question: Are the P+|P, P+|S, and P−|S life cycles consistent with the dynamical amplifier theory? In other words, are these life cycles preceded by a reduced equator-to-pole 2MT gradient and an enhanced equator-to-pole upper-tropospheric temperature gradient?

To answer this question, we examine θ_{2PVU} by area averaging it over two equal-area regions: between the equator and 30°N and between 30° and 90°N. Then, we subtract the high-latitude region from the low-latitude region to calculate $\Delta\theta_{2PVU}$. We perform an identical calculation to derive Δ2MT. Therefore, anomalous high values of $\Delta\theta_{2PVU}$ and Δ2MT represent increases in their respective equator-to-pole temperature gradients. Figure 12a shows $\Delta\theta_{2PVU}$ for each life cycle as a function of lag day. We find that neither the P+|P nor the P+|S life cycle has an enhanced value of $\Delta\theta_{2PVU}$ at negative lags, whereas the P−|S life cycle does. Similarly, Fig. 12b shows that only the P−|S life cycle has an enhanced value of Δ2MT. However, all three life cycles reduce $\Delta\theta_{2PVU}$ and Δ2MT through poleward heat transport. Interestingly, the P+|P life cycle accomplishes this reduction in an environment where $\Delta\theta_{2PVU}$ and Δ2MT are already anomalous low. Therefore, the P+|P and P+|S life cycles are not consistent with the dynamical amplifier theory. Moreover, we cannot conclude that the P−|S life cycle operates in accordance with the dynamical amplifier theory, because although $\Delta\theta_{2PVU}$ is anomalously positive at negative lags, we find that Δ2MT is as well. These results show that in the presence of a reduced equator-to-pole temperature gradient at both the surface and aloft, the PSWs are capable of intense high-latitude poleward heat fluxes. This behavior cannot be explained by the four-box model of Cai (2005, 2006) and its linear parameterization of the

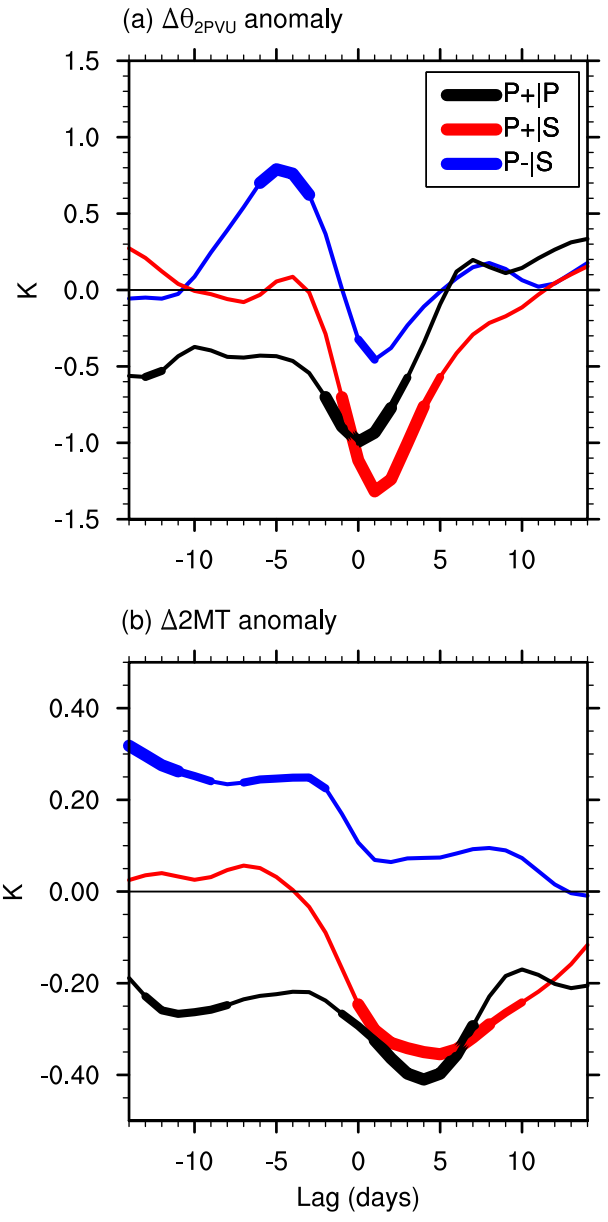

FIG. 12. Composites of anomalous (a) $\Delta\theta_{2PVU}$ and (b) Δ2MT during P+|P (black), P+|S (red), and P−| S (blue) events (n = 34, 44, and 44, respectively). See section 3e for a definition of $\Delta\theta_{2PVU}$ and Δ2MT. A two-sided Student's t test is used to determine statistical significance. The line segments of greatest (medium) thickness indicate significance at the 5% (10%) level. Two iterations of a 1–2–1 smoothing scheme are applied before plotting. Evaluated from ERA-Interim (1979–2014) data.

TABLE 2. Summary of characteristics observed during the P+|P, P+|S, and P−|S life cycles.

Characteristic	Life cycle		
	P+|P	P+|S	P−|S
Energetics			
Arctic 2MT warming?	Yes	Yes	Yes
Anomalously cold Arctic 2MT at negative lags?	No	Yes	Yes
Anomalously warm Arctic 2MT at positive lags?	Yes	Yes	No
Tropical convection and Rossby wave response			
Background ENSO state?	La Niña	Neutral	El Niño
Localized tropical convection over the Maritime Continent?	Yes	Yes	No
Constructive interference with climatological stationary wave?	Yes	Yes	No
E-P flux diagnostics			
Tropical wave activity source?	Yes	Yes	No
Enhanced PSW baroclinic life cycle?	Yes	Yes	No
Enhanced SSW baroclinic life cycle?	No	Yes	Yes
Enhanced polar vortex at negative lags?	Yes	Yes	No
Stratospheric warming?	Yes	Yes	No
Sensible HFC by PSWs over the Arctic?	Yes	Yes	No
Sensible HFC by SSWs over the Arctic?	No	No	Yes
Localized greenhouse effect			
Enhanced TCW over the Arctic?	Yes	Yes	No
Enhanced downward IR over the Arctic?	Yes	Yes	No
Enhanced Arctic 2MT?	Yes	Yes	No
Latent HFC by PSWs over the Arctic?	Yes	Yes	No
Latent HFC by SSWs over the Arctic?	No	No	Yes
Dynamical amplifier theory			
Enhanced equator-to-pole 2MT gradient at negative lags?	No	No	Yes
Enhanced equator-to-pole $\theta_{2\mathrm{PVU}}$ gradient at negative lags?	No	No	Yes
Consistent with dynamical amplifier theory?	No	No	No

flux–gradient relationship. However, it is worth reiterating that we are comparing two processes that occur on vastly different time scales—climatic and subseasonal. In fact, recent studies have warned against the juxtaposition of these two time scales in the context of the Arctic Oscillation versus Arctic amplification (Hassanzadeh et al. 2014; Hassanzadeh and Kuang 2015). These studies argued through modeling work that even though the Arctic Oscillation and Arctic amplification exhibit similar mean states, caution should be used when attributing dynamical processes caused by natural variability to climatic mean states caused by external forcing. It remains to be seen if a similar situation exists between the dynamical amplifier theory and the mechanisms that result in Arctic warming during the PSW life cycles in this study. Our results suggest that future investigation is merited.

4. Conclusions

We summarize the characteristic features of the P+|P, P+|S, and P−|S life cycles in Table 2. The most important conclusion involves a comparison between the P+|S and P−|S life cycles. However, we first discuss the collection of all SSW events (Figs. 2b), which follows the canonical baroclinic life cycle paradigm, with anomalously cold (warm) Arctic temperatures proceeding (following) the peak of the life cycle. One would naturally conclude from this that the SSWs themselves are responsible for the poleward heat transport and thereby warm the Arctic. However, our analyses call this presumption into question. We find that the SSW events with enhanced PSW activity (P+|S) produce more Arctic warming than the SSW events with reduced PSW activity (P−|S). Perhaps even more telling, during the P−|S life cycle the Arctic 2MT never exceeds normal at any lag day (Fig. 2d). We conclude from this that a large fraction of the warm Arctic 2MT found during the SSW life cycle, and the process of warming itself, rests on the amplitude of the PSWs within the life cycle. This finding further supports the tropically excited Arctic warming (TEAM) mechanism, which states that localized tropical convection near the Maritime Continent can amplify the PSWs which leads to sensible and latent heat fluxes into the Arctic, without a reliance on the flux–gradient relationship. As a result of these fluxes, downward IR over the Arctic increases, which warms the 2MT (Doyle et al. 2011; Lee et al. 2011a,b; Yoo et al. 2011, 2012a,b; Lee 2012; Kapsch et al. 2013; Flournoy et al. 2016; Goss et al. 2016).

An additional key aspect of the TEAM mechanism is its reliance on the constructive interference of the PSWs with the climatological stationary waves (BL15; B16; Goss et al. 2016). It has been established in prior studies that when an amplification of the DJFM climatological stationary wave occurs, waves can propagate vertically upward and thereby weaken the stratospheric polar vortex before their influence propagates downward and affects the troposphere (Garfinkel et al. 2010; Fletcher and Kushner 2011; Smith et al. 2010). The initial driving of these PSWs may be tropical convection, but October Eurasian snow cover and Arctic sea ice have been proposed as drivers as well (Cohen et al. 2014; Goss et al. 2016). In this study we show that the PSW life cycles disrupt an anomalously strong stratospheric polar vortex. We observe impressive vertical propagation of PSW activity into the stratosphere, resulting in a rapid weakening of the polar vortex, reminiscent of a sudden stratospheric warming. An anomalously strong polar vortex has been linked to La Niña winters [Butler and Polvani (2011) and references therein]. Moreover, Butler and Polvani (2011) found that sudden stratospheric warmings are statistically as likely to occur during either El Niño or La Niña winters. Because we find that P+|P events most often occur during La Niña winters, further observational analysis and modeling studies are merited into determining the importance of the stratospheric state—to see if it is a necessary condition within the TEAM mechanism.

Finally, the PSW life cycle within the TEAM mechanism appears to be a feasible dynamical pathway capable of sustaining Arctic amplification (Budyko and Izrael 1991; Hoffert and Covey 1992; Miller et al. 2010; Lee 2014). Because the PSW life cycle generally occurs over a 2-week period, it is inherently a subseasonal "weather" event. However, it is not difficult to imagine that a change in frequency of its occurrence would project onto longer, climate time scales. Recent studies have explored this weather–climate relationship. For example, Branstator (2014) found that short-lived pulses of tropical heating can produce long-lived circulation anomalies in the midlatitudes. In examining the error biases of climate models, Ma et al. (2014) showed that they are highly correlated to short-term biases that develop quickly within their integrations as a result of parameterization errors and oftentimes these biases project onto modes of natural variability (Corti et al. 1999). It would be worthwhile to learn more about the dynamical mechanisms of the PSW life cycle through modeling and within the context of the dynamical amplifier theory (Cai 2005, 2006). These studies in turn can lead to the additional benefit of identifying model deficiencies.

Acknowledgments. This study was supported by the National Science Foundation under Grant AGS-1455577. Valuable comments from Michael Goss and Steven Feldstein helped to improve this manuscript. All coding was performed using the National Center for Atmospheric Research Command Language (NCL; NCAR Command Language 2015).

REFERENCES

Baggett, C., and S. Lee, 2015: Arctic warming induced by tropically forced tapping of available potential energy and the role of the planetary-scale waves. *J. Atmos. Sci.*, **72**, 1562–1568, doi:10.1175/JAS-D-14-0334.1.

——, ——, and S. B. Feldstein, 2016: An investigation of the presence of atmospheric rivers over the North Pacific during planetary-scale wave life cycles and their role in Arctic warming. *J. Atmos. Sci.*, **73**, 4329–4347, doi:10.1175/JAS-D-16-0033.1.

Benedict, J. J., S. Lee, and S. B. Feldstein, 2004: Synoptic view of the North Atlantic Oscillation. *J. Atmos. Sci.*, **61**, 121–144, doi:10.1175/1520-0469(2004)061<0121:SVOTNA>2.0.CO;2.

BOM, 2016: Madden-Julian Oscillation (MJO) monitoring. Australian Government Bureau of Meteorology, accessed 10 May 2016. [Available online at http://www.bom.gov.au/climate/mjo/.]

Branstator, G., 2014: Long-lived response of the midlatitude circulation and storm tracks to pulses of tropical heating. *J. Climate*, **27**, 8809–8826, doi:10.1175/JCLI-D-14-00312.1.

Budyko, M. I., and Y. A. Izrael, 1991: *Anthropogenic Climate Change.* University of Arizona Press, 485 pp.

Butler, A. H., and L. M. Polvani, 2011: El Niño, La Niña, and stratospheric sudden warmings: A reevaluation in light of the observational record. *Geophys. Res. Lett.*, **38**, L13807, doi:10.1029/2011GL048084.

Cai, M., 2005: Dynamical amplification of polar warming. *Geophys. Res. Lett.*, **32**, L22710, doi:10.1029/2005GL024481.

——, 2006: Dynamical greenhouse-plus feedback and polar warming amplification. Part I: A dry radiative-transportive climate model. *Climate Dyn.*, **26**, 661–675, doi:10.1007/s00382-005-0104-6.

——, and J.-H. Lu, 2007: Dynamical greenhouse-plus feedback and polar warming amplification. Part II: Meridional and vertical asymmetries of the global warming. *Climate Dyn.*, **29**, 375–391, doi:10.1007/s00382-007-0238-9.

——, and K.-K. Tung, 2012: Robustness of dynamical feedbacks from radiative forcing: 2% solar versus 2 × CO_2 experiments in an idealized GCM. *J. Atmos. Sci.*, **69**, 2256–2271, doi:10.1175/JAS-D-11-0117.1.

Charney, J. G., 1947: The dynamics of long waves in a baroclinic westerly current. *J. Meteor.*, **4**, 136–162, doi:10.1175/1520-0469(1947)004<0136:TDOLWI>2.0.CO;2.

——, and P. G. Drazin, 1961: Propagation of planetary-scale disturbances from the lower into the upper atmosphere. *J. Geophys. Res.*, **66**, 83–109, doi:10.1029/JZ066i001p00083.

Cohen, J., and Coauthors, 2014: Recent Arctic amplification and extreme mid-latitude weather. *Nat. Geosci.*, **7**, 627–637, doi:10.1038/ngeo2234.

Corti, S., F. Molteni, and T. N. Palmer, 1999: Signature of recent climate change in frequencies of natural atmospheric circulation regimes. *Nature*, **398**, 799–802, doi:10.1038/19745.

Dee, D. P., and Coauthors, 2011: The ERA-Interim reanalysis: Configuration and performance of the data assimilation system. *Quart. J. Roy. Meteor. Soc.*, **137**, 553–597, doi:10.1002/qj.828.

Doyle, J. G., G. Lesins, C. P. Thackray, C. Perro, G. J. Nott, T. J. Duck, R. Damoah, and J. R. Drummond, 2011: Water vapor intrusions into the High Arctic during winter. *Geophys. Res. Lett.*, **38**, L12806, doi:10.1029/2011GL047493.

Eady, E. T., 1949: Long waves and cyclone waves. *Tellus*, **1**, 33–52, doi:10.3402/tellusa.v1i3.8507.

ECMWF, 2009: ERA Interim, daily. European Centre for Medium-Range Weather Forecasts public datasets, accessed 25 October 2013. [Available online at http://apps.ecmwf.int/datasets/data/interim-full-daily/levtype=sfc/.]

Edmon, H. J., B. J. Hoskins, and M. E. McIntyre, 1980: Eliassen-Palm cross sections for the troposphere. *J. Atmos. Sci.*, **37**, 2600–2616, doi:10.1175/1520-0469(1980)037<2600:EPCSFT>2.0.CO;2.

Feldstein, S. B., and S. Lee, 2014: Intraseasonal and interdecadal shifts in the Northern Hemisphere: The role of warm pool tropical convection and sea ice. *J. Climate*, **27**, 6497–6518, doi:10.1175/JCLI-D-14-00057.1.

Fletcher, C. G., and P. J. Kushner, 2011: The role of linear interference in the annular mode response to tropical SST forcing. *J. Climate*, **24**, 778–793, doi:10.1175/2010JCLI3735.1.

Flournoy, M. D., S. B. Feldstein, S. Lee, and E. E. Clothiaux, 2016: Exploring the Tropically Excited Arctic Warming Mechanism with station data: Links between tropical convection and Arctic downward infrared radiation. *J. Atmos. Sci.*, **73**, 1143–1158, doi:10.1175/JAS-D-14-0271.1.

Franzke, C., S. B. Feldstein, and S. Lee, 2011: Synoptic analysis of the Pacific–North American teleconnection pattern. *Quart. J. Roy. Meteor. Soc.*, **137**, 329–346, doi:10.1002/qj.768.

Garfinkel, C. I., D. L. Hartmann, and F. Sassi, 2010: Tropospheric precursors of anomalous Northern Hemisphere stratospheric polar vortices. *J. Climate*, **23**, 3282–3299, doi:10.1175/2010JCLI3010.1.

Goss, M., S. B. Feldstein, and S. Lee, 2016: Stationary wave interference and its relation to tropical convection and Arctic warming. *J. Climate*, **29**, 1369–1389, doi:10.1175/JCLI-D-15-0267.1.

Hassanzadeh, P., and Z. Kuang, 2015: Blocking variability: Arctic amplification versus Arctic oscillation. *Geophys. Res. Lett.*, **42**, 8586–8595, doi:10.1002/2015GL065923.

——, ——, and B. F. Farrell, 2014: Responses of midlatitude blocks and wave amplitude to changes in the meridional temperature gradient in an idealized GCM. *Geophys. Res. Lett.*, **41**, 5223–5232, doi:10.1002/2014GL060764.

Hoffert, M. I., and C. Covey, 1992: Deriving global climate sensitivity from paleoclimate reconstructions. *Nature*, **360**, 573–576, doi:10.1038/360573a0.

Hoskins, B. J., and D. J. Karoly, 1981: The steady linear response of a spherical atmosphere to thermal and orographic forcing. *J. Atmos. Sci.*, **38**, 1179–1196, doi:10.1175/1520-0469(1981)038<1179:TSLROA>2.0.CO;2.

Hovmöller, E., 1949: The trough-and-ridge diagram. *Tellus*, **1**, 62–66, doi:10.1111/j.2153-3490.1949.tb01260.x.

Kapsch, M.-L., R. G. Graversen, and M. Tjernström, 2013: Springtime atmospheric energy transport and the control of Arctic summer sea-ice extent. *Nat. Climate Change*, **3**, 744–748, doi:10.1038/nclimate1884.

Lee, S., 2012: Testing of the Tropically Excited Arctic Warming Mechanism (TEAM) with traditional El Niño and La Niña. *J. Climate*, **25**, 4015–4022, doi:10.1175/JCLI-D-12-00055.1.

——, 2014: A theory for polar amplification from a general circulation perspective. *Asia-Pac. J. Atmos. Sci.*, **50**, 31–43, doi:10.1007/s13143-014-0024-7.

——, S. B. Feldstein, D. Pollard, and T. S. White, 2011a: Do planetary wave dynamics contribute to equable climates? *J. Climate*, **24**, 2391–2404, doi:10.1175/2011JCLI3825.1.

——, T. Gong, N. Johnson, S. B. Feldstein, and D. Pollard, 2011b: On the possible link between tropical convection and the Northern Hemisphere Arctic surface air temperature change between 1958 and 2001. *J. Climate*, **24**, 4350–4367, doi:10.1175/2011JCLI4003.1.

Lorenz, E. N., 1955: Available potential energy and the maintenance of the general circulation. *Tellus*, **7**, 157–167, doi:10.3402/tellusa.v7i2.8796.

Lu, J.-H., and M. Cai, 2010: Quantifying contributions to polar warming amplification in a coupled general circulation model. *Climate Dyn.*, **34**, 669–687, doi:10.1007/s00382-009-0673-x.

Ma, H.-Y., and Coauthors, 2014: On the correspondence between mean forecast errors and climate errors in CMIP5 models. *J. Climate*, **27**, 1781–1798, doi:10.1175/JCLI-D-13-00474.1.

Madden, R. A., and P. R. Julian, 1971: Detection of a 40–50 day oscillation in the zonal wind in the tropical Pacific. *J. Atmos. Sci.*, **28**, 702–708, doi:10.1175/1520-0469(1971)028<0702:DOADOI>2.0.CO;2.

——, and ——, 1972: Description of global-scale circulation cells in the tropics with a 40–50 day period. *J. Atmos. Sci.*, **29**, 1109–1123, doi:10.1175/1520-0469(1972)029<1109:DOGSCC>2.0.CO;2.

Miller, G. H., R. B. Alley, J. Brigham-Grette, J. J. Fitzpatrick, L. Polyak, M. C. Serreze, and J. W. C. White, 2010: Arctic amplification: Can the past constrain the future? *Quat. Sci. Rev.*, **29**, 1779–1790, doi:10.1016/j.quascirev.2010.02.008.

NCAR Command Language, 2015: NCL version 6.3.0. UCAR/NCAR, Computational and Information Systems Laboratory. [Available online at https://www.ncl.ucar.edu/prev_releases.shtml.]

Newman, M., G. N. Kiladis, K. M. Weickmann, F. M. Ralph, and P. D. Sardeshmukh, 2012: Relative contributions of synoptic and low-frequency eddies to time-mean atmospheric moisture transport, including the role of atmospheric rivers. *J. Climate*, **25**, 7341–7361, doi:10.1175/JCLI-D-11-00665.1.

NOAA/NCEP/CPC, 2016: Cold & warm episodes by season. National Centers for Environmental Prediction/Climate Prediction Center, accessed 24 October 2016. [Available online at http://www.cpc.ncep.noaa.gov/products/analysis_monitoring/ensostuff/ensoyears.shtml.]

Panofsky, H. A., and J. A. Dutton, 1984: *Atmospheric Turbulence: Models And Methods for Engineering Applications.* Wiley, 397 pp.

Peixoto, J. P., and A. H. Oort, 1974: The annual distribution of atmospheric energy on a planetary scale. *J. Geophys. Res.*, **79**, 2149–2159, doi:10.1029/JC079i015p02149.

——, and ——, 1992: *Physics of Climate.* American Institute of Physics, 520 pp.

Sardeshmukh, P. D., and B. J. Hoskins, 1988: The generation of global rotational flow by steady idealized tropical divergence. *J. Atmos. Sci.*, **45**, 1228–1250, doi:10.1175/1520-0469(1988)045<1228:TGOGRF>2.0.CO;2.

Smith, K. L., C. G. Fletcher, and P. J. Kushner, 2010: The role of linear interference in the annular mode response to extratropical surface forcing. *J. Climate*, **23**, 6036–6050, doi:10.1175/2010JCLI3606.1.

Trenberth, K. E., and D. P. Stepaniak, 2003: Covariability of components of poleward atmospheric energy transports on

seasonal and interannual timescales. *J. Climate*, **16**, 3691–3705, doi:10.1175/1520-0442(2003)016<3691:COCOPA>2.0.CO;2.

Wheeler, M. C., and H. H. Hendon, 2004: An all-season real-time multivariate MJO index: Development of an index for monitoring and prediction. *Mon. Wea. Rev.*, **132**, 1917–1932, doi:10.1175/1520-0493(2004)132<1917:AARMMI>2.0.CO;2.

Wu, Y., M. Ting, R. Seager, H.-P. Huang, and M. A. Cane, 2011: Changes in storm tracks and energy transports in a warmer climate simulated by the GFDL CM2.1 model. *Climate Dyn.*, **37**, 53–72, doi:10.1007/s00382-010-0776-4.

Yoo, C., S. B. Feldstein, and S. Lee, 2011: The impact of the Madden-Julian Oscillation trend on the Arctic amplification of surface air temperature during the 1979–2008 boreal winter. *Geophys. Res. Lett.*, **38**, L24804, doi:10.1029/2011GL049881.

——, S. Lee, and S. B. Feldstein, 2012a: Arctic response to an MJO-like tropical heating in an idealized GCM. *J. Atmos. Sci.*, **69**, 2379–2393, doi:10.1175/JAS-D-11-0261.1.

——, ——, and ——, 2012b: Mechanisms of Arctic surface air temperature change in response to the Madden–Julian oscillation. *J. Climate*, **25**, 5777–5790, doi:10.1175/JCLI-D-11-00566.1.

Zelinka, M. D., and D. L. Hartmann, 2012: Climate feedbacks and their implications for poleward energy flux changes in a warming climate. *J. Climate*, **25**, 608–624, doi:10.1175/JCLI-D-11-00096.1.